SCIENCE CHINA
Chemistry

•ARTICLES•
SPECIAL ISSUE: 2023 Emerging Investigator Issue

December 2023 Vol.66 No.12: 3525–3531
https://doi.org/10.1007/s11426-023-1777-y

An anthraquinone-based Cu(I) cyclic trinuclear complex for photo-catalyzing C–C coupling reactions

Yu-Mei Wang, Kai-Ming Mo, Xiao Luo, Ri-Qin Xia, Jing-Yi Song, Guo-Hong Ning* & Dan Li

College of Chemistry and Materials Science, Guangdong Provincial Key Laboratory of Functional Supramolecular Coordination Materials and Applications, Jinan University, Guangzhou 510632, China

Received August 8, 2023; accepted August 23, 2023; published online November 22, 2023

Development of transition metal-based photocatalysts with low cost, strong visible light absorption, and high efficiency is a long-stand pursuit for advanced organic synthesis, yet remains highly challenging. In this article, an anthraquinone-based copper(I) cyclic trinuclear complex (**1**) was designed and it featured strong visible light absorption, high charge separation efficiency and photochemical properties. Complex **1** as a heterogeneous photocatalyst can efficiently catalyze homo-coupling of terminal alkynes and denitrification-oxidative coupling reaction between hydrazinopyridine and terminal alkynes with excellent yield (up to 99%), broad substrate tolerance (27 examples) and superior reusability (up to 10 cycles without loss of performance) under mild conditions.

cyclic trinuclear complex, photocatalysis, C–C coupling reaction

Citation: Wang YM, Mo KM, Luo X, Xia RQ, Song JY, Ning GH, Li D. An anthraquinone-based Cu(I) cyclic trinuclear complex for photo-catalyzing C–C coupling reactions. *Sci China Chem*, 2023, 66: 3525–3531, https://doi.org/10.1007/s11426-023-1777-y

1 Introduction

With the increasing global consumption of non-renewable fossil fuels, the development of a sustainable, environmentally friendly and efficient energy supply is in great demand and has become one of the major challenges [1,2]. Among the various clean energy sources, solar energy is attractive, and tremendous progress has been achieved in its storage and transformation. Especially, solar energy can be absorbed by a photocatalyst whose excited state is able to catalyze organic transformation [3–6]. In the past decades, many metal complexes have been prepared and used as photocatalysts; however, most of them are based on expensive noble metals including ruthenium (Ru) and iridium (Ir) [7–12]. Besides high cost and scarcity, these complexes are suffering from weak visible-light absorption, and poor photostability, which hinder the further improvement of photocatalytic efficiency and their applications. Therefore, the design of photocatalysts composed of low-cost and earth-abundant metals with strong visible-light absorption, excellent photochemical stability and appropriate oxidation-reduction potential are highly desired, yet remains a great challenge.

Due to the high abundance, low price and toxicity, high reactivity and low standard reduction potential of copper (Cu) [13], Cu-based metal complexes can be a promising alternative option for photocatalysis [14–16]. For instance, Cu(I) complexes bearing phosphines or phenanthrolines ligands can act as photocatalysts to promote several organic transformations [17–19]. However, these Cu(I) complexes usually display low molar extinction coefficients ($\varepsilon < 3{,}000$ M^{-1} cm^{-1}) in the visible range, limiting their photocatalytic activities [20]. To address these issues, the introduction of organic chromophores, such as boron dipyrromethene (BODIPY), into Cu(I) complexes can effectively improve their visible-light absorption, leading to significant en-

*Corresponding author (email: guohongning@jnu.edu.cn)

hancement of photocatalytic activities [21,22]. Unfortunately, the intricate and multistep syntheses of BODIPY ligand largely increase the cost of such Cu(I)-based photocatalysts and lower its accessibility. Moreover, Cu(I)-based photocatalysts are generally soluble in most organic solvents, resulting in difficulty in catalyst recovery.

Unlike the conventionally distorted tetrahedral and saturated four-coordinate structure, each Cu(I) ion in copper-based cyclic trinuclear complexes (Cu-CTCs) features a linear and unsaturated two-coordinate conformation, leading to interesting application in the fields of photoluminescence (PL), optoelectronics, host-guest chemistry and catalysis [23–28]. Recently, our studies demonstrated that the modification of pyrazole ligands remarkably altered the properties of Cu-CTCs [29–31]. Anthraquinone (AQ) and its derivatives as classic organic photocatalysts are widely used for various chemical reactions including photo-oxygen activation and hydrogen atom transfer [32–36]. Thus, we envisioned that the incorporation of the AQ motif into Cu-CTCs would improve the light absorption ability and photocatalytic activity. Importantly, AQ-based pyrazole ligands are much cheaper than BODIPY ligands.

Herein, we designed an AQ-based Cu-CTC (**1**) from anthraquinone-based pyrazole ligand (**HL**) and $Cu(NO_3)_2{\cdot}3H_2O$ (Scheme 1). For comparison, a reference Cu-CTC (**2**) without AQ groups was prepared (Scheme S2, Supporting Information online). The introduction of AQ groups significantly enhanced the light absorption ability and complex **1** exhibited a high molar extinction coefficient (ε) of 2.44×10^5 M^{-1} cm^{-1} at 249 nm (Table S1, Supporting Information online) in a dichloromethane (DCM) solution, which is ca. 59-fold and 8-fold larger than those of **2** and **HL**, respectively. In addition, in solid-state, complex **1** also exhibited a wide range of light absorption (200–600 nm), good charge separation efficiency and excellent ability to generate reactive oxygen species (*e.g.*, $O_2^{\bullet-}$ and $^1O_2$). Interestingly, complex **1** delivered excellent photocatalytic activities for C–C coupling reactions including homo-coupling of terminal alkynes (12 examples, yield up to 99) as well as denitrification-oxidative coupling reaction between hydrazinopyridine and terminal alkynes (15 examples, yield up to 99). Notably, Cu-CTC **1** as a heterogeneous photocatalyst displayed superior stability and can be reused 10 times without loss of catalytic performance.

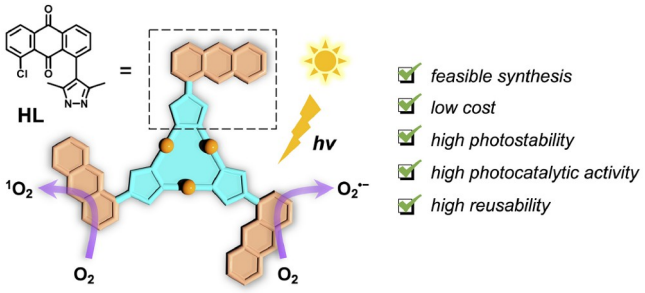

Scheme 1 Schematic demonstration of AQ-based Cu-CTCs. Orange balls represent Cu(I) ions (color online).

2 Results and discussion

2.1 Structure and characterization

The anthraquinone-based pyrazolyl ligand (**HL**) was newly prepared in gram scale from 1,8-dichloroanthracene-9,10-dione, a low-cost and commercially available chemical (0.17 US dollar/g), *via* the Suzuki-Miyaura cross-coupling reactions (Scheme S1 and see Supporting Information online for details). The structure of **HL** was confirmed by nuclear magnetic resonance (NMR), mass spectrometer (MS) and single crystal X-ray diffraction (SCXRD) analysis (Figures S1 and S7). A mixture of $Cu(NO_3)_2{\cdot}3H_2O$, **HL**, and triethylamine in acetonitrile (MeCN) under solvothermal conditions afforded AQ-based CTC (**1**) as reddish-brown platelet crystals, which were suitable for SCXRD analysis (See Supporting Information online for details). For comparison, Cu-CTC (**2**) was prepared from the 3,5-dimethylpyrazole ligand and $Cu(NO_3)_2{\cdot}3H_2O$ (See Scheme S2 and Supporting Information online for details). The SCXRD analysis reveals that **1** crystallizes in the triclinic crystal system with a space group of *P*-1 and CTC unit with a nine-membered Cu_3N_6 features an ideal planar configuration in the asymmetric unit (Figure 1a). In addition, the dihedral angle between the AQ motif and Cu_3N_6 plane is 120°, and a dimer is formed between two neighboring CTC units through π-π interaction with a short Cu–Cu distance of 2.83 Å, which was commonly observed in reported Cu-CTCs (Figure 1b) [22]. Moreover, the multiple π-π interactions are observed in the crystal including face-to-face and parallel displaced shaped stacking between two neighboring anthraquinone motifs with distances ranging from 3.38 to 3.62 Å (Figure 1c, d), as well as the tight stacking between anthraquinone and CTC unit with a distance of 3.47 Å (Figure 1e). Such π-π interactions might promote electron transport in the crystals of **1** [37], which makes it possible to serve as a promising photocatalyst. The thermal stability and the phase purity of **1** were confirmed by thermogravimetric analyses (TGA) and powder X-ray diffraction (PXRD) (Figure S3). XPS analysis suggested that Cu ions were monovalent in **1** (Figure S4).

2.2 Optics and electrochemistry

Complex **1** exhibited a high molar extinction coefficient (ε) of 2.44×10^5 M^{-1} cm^{-1} at 249 nm in DCM solution (Table S1), which is ca. 59-fold and 8-fold higher than that of **2** and **HL**, respectively. Besides strong light absorption in solution, the reddish-brown colored crystals of **1** also indicate it has strong visible-light absorbing ability in solid-state. As shown in

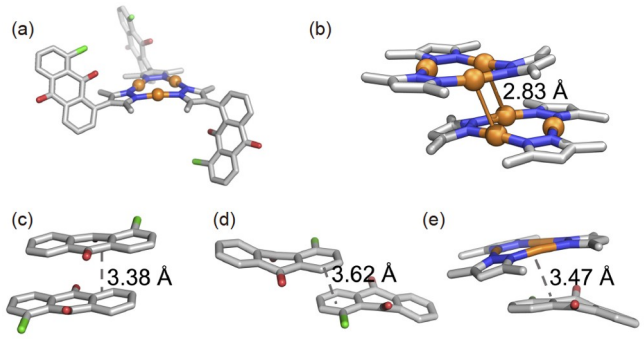

Figure 1 (a) Crystal structures of **1**. (b) Side view showing an interdimer Cu···Cu distance of 2.83 Å. (c–e) π-π interactions in the stacking structure of **1** (color online).

Figure 2a, the solid-state ultraviolet-visible (UV/Vis) diffuse reflectance spectroscopy of **HL** and **1** revealed that they both absorbed light in the 200 to 600 nm region, while **2** only absorbed light in the 200 to 400 nm region. This suggested the induction of the AQ motif largely improved the visible-light absorbing ability of Cu-CTC. In addition, the optical band gap (E_g) of **HL**, **1** and **2** was estimated to be approximately 1.91, 1.71 and 2.67 eV (Figure 2b and Figure S6a–c), respectively, using the Tauc plot method. The Mott-Schottky experiments determined the flat band potentials of **HL**, **1** and **2** were determined to be −0.61, −0.67 and −0.92 eV *vs*. Ag/AgCl at pH 6.8, respectively (Figures S6d–f), which were equal to their conduction band (CB) potentials. Afterward, valence band (VB) potentials of **HL**, **1** and **2** could be estimated to be 1.30, 1.04 and 1.75 eV *vs*. Ag/AgCl at pH 6.8 (Figure 2b), on account of the band gap energy equation. As shown in Figure 2c, the electrochemical impedance spectroscopy (EIS) of **HL**, **1** and **2** showed a semicircle, but the diameter of **1** was much smaller than those of **HL** and **2**, indicating that the charge transfer resistance of **1** was the lowest and the charge separation efficiency was the highest compared with **HL** and **2**. Moreover, the transient photocurrent measurement in Figure 2d showed that the photocurrent density of **1** was larger than those of **HL** and **2**, indicating that **1** had the best effective spatial separation ability of photogenerated charge carriers. Furthermore, electron paramagnetic resonance (EPR) experiments of **1** were performed to probe its ability to activate oxygen under visible light irradiation. As shown in Figure 2e, f, in the presence of the radical trapping reagents such as 5,5-dimethyl-1-pyrroline *N*-oxide (DMPO) and 2,2,6,6-tetramethylpiperidone (TEMP), the EPR signals were observed upon the white light irradiation of **1** in air, implying the generation of superoxide radical anion ($O_2^{\bullet-}$) and singlet oxygen ($^1O_2$). These experiments illustrate that **1** is a potential excellent catalyst for photocatalytic oxidation reactions.

2.3 Photocatalytic oxidative C–C coupling reaction

2.3.1 Homo-coupling reaction of terminal alkynes

1,3-Diynes as important components are widely present in natural products and extensively used in the pharmaceutical industry and material science [38,39]. Conventionally, the preparation of 1,3-diynes using copper-based catalysts required relatively harsh reaction conditions such as high temperature, and strong base [40–42]. Therefore, it is desired to develop new catalysts to prepare the 1,3-diynes under mild conditions. Recently, it has been found that Cu-CTC units can activate C–H bonds of terminal alkynes [43–45]. Therefore, we have tested the photocatalytic activity of **1** for the synthesis of 1,3-diynes. The reaction conditions were optimized using homo-coupling of phenylacetylene (**3a**) as a

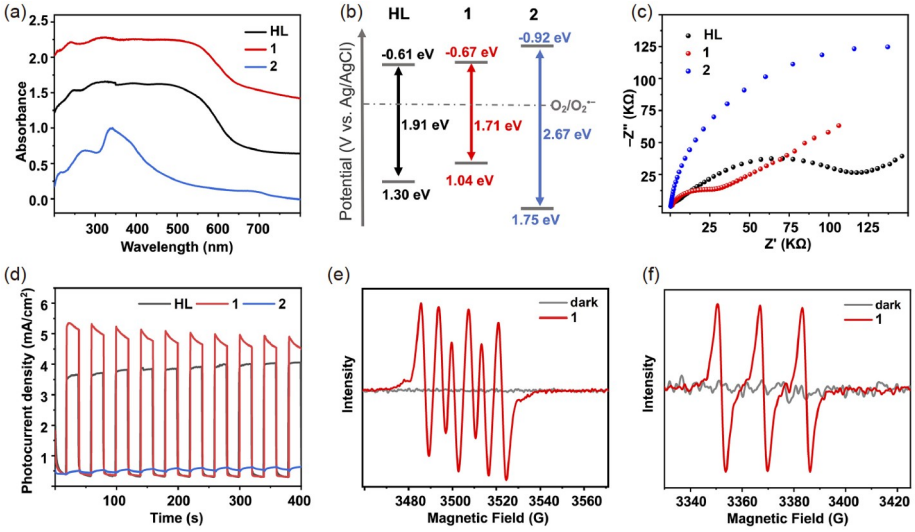

Figure 2 (a) UV-Vis diffuse reflectance spectra; (b) schematic diagram of the optical band gap; (c) photocurrent response curves and (d) EIS Nyquist plots of **1**, **2** and HL. EPR spectra of **1** in the presence of (e) DMPO or (f) TEMP before and after light irradiation (color online).

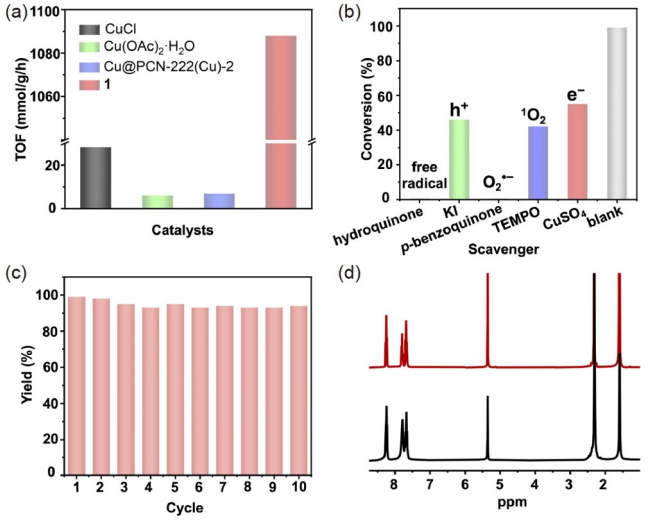

Figure 3 (a) Comparison of the photocatalytic efficiency of four reprehensive Cu-based catalysts. (b) Effects of scavengers on homo-coupling reaction of **3a** under standard reaction conditions. (c) Recycling experiments with **1** as the photocatalyst for the homo-coupling reaction of **3a**. (d) ^{1}H NMR spectra of freshly prepared **1** (black) and recovered **1** after photocatalytic homo-coupling reaction of **3a** (red) (color online).

model reaction. As shown in Table 1, the reaction could not proceed without **1**, and the optimal catalytic **1** content was 0.5 mol% of the substrate. Replacing the methanol with tetrahydrofuran (THF), DCM or MeCN greatly reduced the reaction conversion (Table 1, entries 3–5). The reaction cannot take place in the absence of oxygen, light, and usage of **HL**, $Ir(ppy)_3$ or $Ru(ppy)_3Cl_2$ instead of **1** (Table 1, entries 6–11). When **2**, or CuI was employed as a catalyst instead of **1**, the yields were remarkably reduced to 32% or 14% (Table 1, entries 12–13). When the ligand **HL** was physically mixed with **2** or CuI as catalysts, the conversion decreased to 45% and 25% (Table 1, entries 14–15). These results show that the anthraquinone ligand and copper ions play synergistic effects. To further evaluate the photocatalytic activity of **1**, a large-scale reaction involving 5 mmol of **3a** with low catalyst loading (0.016 mol% **1**) was conducted. Notably, the 1,3-diynes products (**4a**) can be obtained with 87% conversion (Table 1, entry 16), suggesting high photocatalytic activity of **1**. The turnover frequency (TOF) value of **1** was 1,088 mmol g^{-1} h^{-1} and was 2−6 orders of magnitude greater than that of other reported Cu-based catalysts for self-coupling reactions of **3a** (Figure 3a and Table S3).

Under optimized reaction conditions, a series of terminal alkynes were explored, and the results are listed in Table 2. For aryl alkynes, the corresponding self-coupling products were obtained in relatively high yields, which ranged from 93% to 99%, regardless of the electron-donating groups or the electron-withdrawing groups. Generally, the stronger the electron-withdrawing ability of the substituent, the higher conversion yields were obtained. The reaction efficiency of naphthyl (98% yield for **3j**) with a large conjugated aromatic

Table 1 Screening of synthetic conditions for 1,4-diphenylbutadiyne[a)]

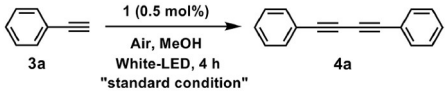

Entry	Change from the "standard condition"	Conversion (%)
1	none	>99
2	No **1**	NR
3	DCM instead MeOH	28
4	MeCN instead MeOH	trace
5	THF instead MeOH	20
6	No light	NR
7	O_2 instead Air	>99
8	N_2 instead Air	NR
9	**HL** instead **1**	NR
10	$Ir(ppy)_3$	NR
11	$Ru(ppy)_3Cl_2$	NR
12	**2** instead **1**	32
13	CuI instead **1**	14
14	**HL**+ **2** instead **1**	45
15	**HL**+ CuI instead **1**	25
16 [b)]	5 mmol **3a**	87

a) Reaction conditions: phenylacetylene (0.5 mmol), **1** (0.0025 mmol), MeOH (2 mL), air, 12 W white lamp, room temperature, 4 h. Conversion of phenylacetylen was determined by gas chromatograph-mass spectrometer (GC-MS) analysis. b) **3a** (5 mmol), **1** (1 mg, 0.84 μmol).

Table 2 Substrate expansion of 1,3-diyne[a)]

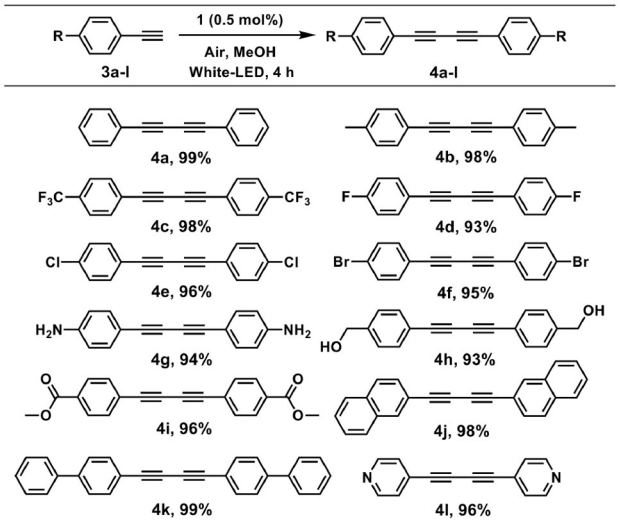

a) Reaction conditions: **3** (0.5 mmol), **1** (0.0025 mmol, 3 mg), MeOH (2 mL), air, 12 W white lamp, room temperature, 4 h. Isolated yields are presented here.

structural substituent or biphenyl (99% yield for **3k**) groups is comparable to that of phenyl groups. In addition, complex

1 also effectively photocatalyzed the self-coupling of alkyne-bearing aromatic heterocyclic substituents (**3l**) with a high yield of 96%. These results prove that **1** is an excellent photocatalyst for the homo-coupling of aromatic terminal alkynes.

2.3.2 Denitrogenation oxidative coupling of hydrazinylpyridines with terminal alkynes

The high photocatalytic activity of **1** encourages us to further explore other C–C coupling reactions of terminal alkynes. The C–N bond cleavage is crucial in organic synthesis, but it is less explored, especially for less active C–N bonds such as amines and hydrazides, due to their high bond dissociation energy [46,47]. Therefore, the Cu-CTC **1** photocatalyzed denitrogenation coupling of 2-hydrazinopyridines with terminal alkynes to form 2-(alkyl/aryl)pyridines was attempted [48]. The reaction condition was optimized using **3a** and 2-hydrazinopyridine (**5a**) as model compounds (Table 3). Experiments have shown that the reaction cannot proceed without any one of the bases, catalysts, light and oxygen (Table 3, entries 2–5). The reaction did not take place when the solvent was changed to THF or MeCN (Table 3, entries 6–7). The reaction did not occur when **HL**, $Ir(ppy)_3$ or $Ru(ppy)_3Cl_2$ was used as the catalyst (Table 3, entries 8–10).

Table 3 Screening of synthetic conditions for 2-(phenylethynyl)pyridine[a)]

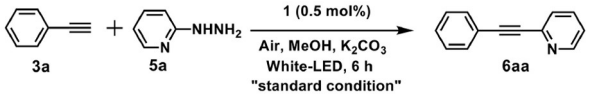

Entry	Change from the "standard condition"	Conversion (%)
1	none	>99
2	No **1**	NR
3	No light	NR
4	No base	NR
5	N_2 instead Air	NR
6	THF instead MeOH	NR
7	MeCN instead MeOH	NR
8	**HL** instead **1**	NR
9	$Ir(ppy)_3$	NR
10	$Ru(ppy)_3Cl_2$	NR
11	CuCl instead **1**	41
12	**2** instead **1**	40
13	**HL** + **2** instead **1**	71
14	**HL** +CuCl instead **1**	55
15[b)]	5 mmol **3a**	53

a) Reaction conditions: phenylacetylene (0.5 mmol), 2-hydrazinopyridine (0.5 mmol), **1** (0.0025 mmol), K_2CO_3 (0.6 eq.), MeOH (2 mL), air, 12 W white lamp, room temperature, 6 h. Conversion of phenylacetylene was determined by GC-MS analysis. b): **3a** (5 mmol), **5a** (5 mmol), **1** (1 mg 0.84 μmol).

When CuCl or **2** were used as catalysts, the conversions were 41% or only 40% (Table 3, entries 11–12). When **HL** was physically mixed with CuCl or **2** as catalysts, the conversion was 55% or 71% (Table 3, entries 13–14). Based on these results, the conditions were optimized as follows: 0.5 mol% **1** as the catalyst, and 0.6 equiv. K_2CO_3 as base in MeOH (2 mL) for 6 h at rt under air atmosphere.

The scope of the substrate was explored using the optimized condition. As shown in Table 4, the reactivity of alkynes with different groups was screened, and the corresponding oxidative coupling products can be obtained in high yields. Notably, the conversion of aryl alkynes (from 90% to 99%) was significantly higher than those of alkyl alkynes (up to 88%). The alkynes with electron-donating (**3b**) or -withdraw groups (**3c**–**3f**), did not alter the yield of coupling products. In addition, the alkynes with heterocyclic substitutes (**3l** and **3m**) also gave coupling products with high yields of 96% and 94%, respectively. The alkynes with extended conjugated substituents (**3j** and **3k**) exhibited slightly lower conversion (90% and 92% yields for **6ja** and **6ka**, respectively) compared with others. Finally, the reactivity of 2-hydrazinopyridines derivatives was also tested. Specifically, excellent yields can be obtained from the methyl (**5b**) and bromide substituted (**5c**) 2-hydrazinopyridines. Thus, **1** is a distinguished photocatalyst to catalyze denitrification-oxidative coupling of 2-hydrazinopyridines and terminal alkynes.

2.4 Reaction mechanisms and recyclability tests

To probe the reaction mechanisms, several control experiments were conducted. Specifically, after adding hydro-

Table 4 Substrate expansion of 2-(phenylethynyl)pyridine[a)]

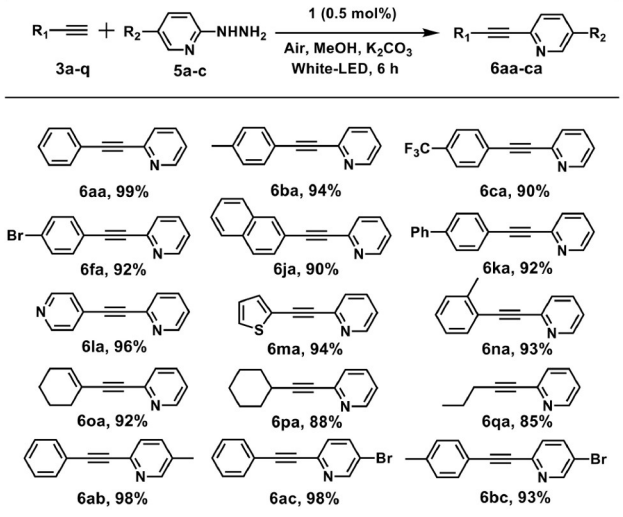

a) Reaction conditions: **3** (0.5 mmol), **5** (0.5 mmol), **1** (0.0025 mmol, 3 mg), K_2CO_3 (0.3 mmol), MeOH (2 mL), air, 12 W white lamp, room temperature, 6 h. Isolated yields are presented here.

quinone (HQ), a scavenger for free radicals, or *p*-benzoquinone (BQ), a scavenger for $O_2^{\bullet-}$, the homo-coupling of **3a** is completely inhibited, indicating that $O_2^{\bullet-}$ is involved in the reaction process (Figure 3b). The addition of the scavengers for holes (KI), electrons ($CuSO_4$) or $^1O_2$ (2,2,6,6-tetramethylpiperidinooxy (TEMPO)), slightly decreases the yields of reactions, suggesting the holes, electrons and $^1O_2$ can be ruled out from the reaction pathway. Similarly, the reaction mechanism of denitrogenation oxidative coupling was also examined. Specifically, with the addition of HQ, or TEMPO, the denitrogenation coupling reaction is completely inhibited, indicating that $^1O_2$ is the main active species involved in the catalytic cycles (Figure S9a). In addition, the reaction is also completely inhibited after adding $CuSO_4$, indicating that electron transfer also occurs during the catalytic cycles (Figure S9a). When adding the KI or BQ, the yields of reactions are slightly decreased, implying the hole and $O_2^{\bullet-}$ are not involved. Based on the control experiments and the previously reported examples [41,48,49], the reaction mechanisms of homo-coupling and denitrogenation oxidative coupling reaction photocatalyzed by **1** is proposed and is shown in Figures S8 and S10 (See Supporting Information online for details).

The stability of **1** during the photocatalytic cycles was examined. Generally, the crystals of **1** were recovered by centrifugation and washing with MeOH, and then were used for the next catalytic runs. Interestingly, for the homo-coupling reaction, the PXRD of **1** after 10 cycles exhibited identical peaks with decreased intensity compared to as-prepared crystals of **1** (Figure S11b). Meanwhile, ^{1}H NMR spectra of **1** after 10 cycles displayed identically characteristic signals (Figure 3d). These results confirmed that the structural integrity of **1** remains intact during the photocatalytic cycles, and the slightly decreased crystallinity might be due to the stirring. Similarly, for the denitrogenation oxidative coupling reaction, after 5 runs, complex **1** remains intact evidenced by PXRD and ^{1}H NMR analysis (Figure S11). More importantly, the photocatalytic performance of **1** did not noticeably change after 10 runs (Figure 3c). These results demonstrate the prominent stability and reusability of **1** as a heterogeneous photocatalyst.

3 Conclusions

In summary, we successfully prepared an anthraquinone-based Cu-CTC (**1**) from readily accessible sources with low cost. Complex **1** delivered strong light absorption ability either in solution or in solid-state, and exhibited high charge separation efficiency as well as excellent photochemical properties, endowing the activation of oxygen to $O_2^{\bullet-}$ and $^1O_2$ under light irradiation. Owing to these merits of **1**, we demonstrated that **1** can efficiently photocatalyze homo-coupling and the denitrification-oxidative coupling reaction of terminal alkynes with broad substrate compatibility (27 examples), excellent yields (up to 99%), and superior reusability (up to 10 runs without loss of catalytic performance) under mild conditions. This study provides a new paradigm for the construction of efficient copper-based photocatalysts for advanced organic synthesis.

Acknowledgements Guo-Hong Ning is thankful for the support from the Guangdong Basic and Applied Basic Research Foundation (2019B151502024) and the Guangzhou Science and Technology Project (202201020038). This work was supported by the National Natural Science Foundation of China (22371091, 21975104, 22150004, 22101099) and the Guangdong Major Project of Basic and Applied Research (2019B030302009).

Conflict of interest The authors declare no conflict of interest.

Supporting information The supporting information is available online at chem.scichina.com and link.springer.com/journal/11426. The supporting materials are published as submitted, without typesetting or editing. The responsibility for scientific accuracy and content remains entirely with the authors.

1 Lv H, Geletii YV, Zhao C, Vickers JW, Zhu G, Luo Z, Song J, Lian T, Musaev DG, Hill CL. *Chem Soc Rev*, 2012, 41: 7572–7589
2 Kim D, Sakimoto KK, Hong D, Yang P. *Angew Chem Int Ed*, 2015, 54: 3259–3266
3 Li J, Yuan H, Zhang W, Jin B, Feng Q, Huang J, Jiao Z. *Carbon Energy*, 2022, 4: 294–331
4 Qiu X, Zhang Y, Zhu Y, Long C, Su L, Liu S, Tang Z. *Adv Mater*, 2021, 33: 2001731
5 Chang P, Wang Y, Wang Y, Zhu Y. *Chem Eng J*, 2022, 450: 137804
6 Gao C, Wang J, Xu H, Xiong Y. *Chem Soc Rev*, 2017, 46: 2799–2823
7 Wang P, Guo S, Wang HJ, Chen KK, Zhang N, Zhang ZM, Lu TB. *Nat Commun*, 2019, 10: 3155
8 Takizawa S, Ikuta N, Zeng F, Komaru S, Sebata S, Murata S. *Inorg Chem*, 2016, 55: 8723–8735
9 Zhang N, Chen KK, Guo S, Wang P, Zhang M, Zhao J, Zhang ZM, Lu TB. *Appl Catal B-Environ*, 2019, 253: 105–110
10 Guo S, Chen KK, Dong R, Zhang ZM, Zhao J, Lu TB. *ACS Catal*, 2018, 8: 8659–8670
11 Wang P, Dong R, Guo S, Zhao J, Zhang ZM, Lu TB. *Natl Sci Rev*, 2020, 7: 1459–1467
12 Wei S, Liang H, Dao A, Xie Y, Cao F, Ren Q, Yadav AK, Kushwaha R, Mandal AA, Banerjee S, Zhang P, Ji S, Huang H. *Sci China Chem*, 2023, 66: 1482–1488
13 Wang Y, Lin X, Mo K, Xie M, Huang Y, Ning G, Li D. *Angew Chem*, 2023, 135: e202218369
14 Wenger OS. *J Am Chem Soc*, 2018, 140: 13522–13533
15 Wang E, Chen K, Chen Y, Zhang J, Lin X, Chen M. *Sci China Chem*, 2021, 64: 17–21
16 Hernandez-Perez AC, Collins SK. *Acc Chem Res*, 2016, 49: 1557–1565
17 Mara MW, Fransted KA, Chen LX. *Coord Chem Rev*, 2015, 282-283: 2–18
18 Forero Cortés PA, Marx M, Trose M, Beller M. *Chem Catal*, 2021, 1: 298–338
19 Zhong M, Pannecoucke X, Jubault P, Poisson T. *Beilstein J Org Chem*, 2020, 16: 451–481
20 Zhang Y, Schulz M, Wächtler M, Karnahl M, Dietzek B. *Coord Chem Rev*, 2018, 356: 127–146
21 Chen KK, Qin CC, Ding MJ, Guo S, Lu TB, Zhang ZM. *Proc Natl Acad Sci USA*, 2022, 119: e2213479119

22 Xia RQ, Zheng J, Wei RJ, He J, Ye DQ, Li MD, Ning GH, Li D. *Inorg Chem Front*, 2022, 9: 2928–2937
23 Dias HVR, Diyabalanage HVK, Eldabaja MG, Elbjeirami O, Rawashdeh-Omary MA, Omary MA. *J Am Chem Soc*, 2005, 127: 7489–7501
24 Ni WX, Li M, Zheng J, Zhan SZ, Qiu YM, Ng SW, Li D. *Angew Chem Int Ed*, 2013, 52: 13472–13476
25 Zhang ZY, Ye DQ, Gao QQ, Shi ZC, Xie M, Zhan SZ, Huang YL, Ning GH, Li D. *Inorg Chem Front*, 2021, 8: 2299–2304
26 Shi ZC, Chen W, Zhan SZ, Li M, Xie M, Li YY, Ng SW, Huang YL, Zhang Z, Ning GH, Li D. *Inorg Chem Front*, 2020, 7: 1437–1444
27 Larionov VA, Stashneva AR, Titov AA, Lisov AA, Medvedev MG, Smol'yakov AF, Tsedilin AM, Shubina ES, Maleev VI. *J Catal*, 2020, 390: 37–45
28 Patterson MR, Dias HVR. *Dalton Trans*, 2022, 51: 375–383
29 Lin X, Wang Y, Chen X, You P, Mo K, Ning G, Li D. *Angew Chem Int Ed*, 2023, 62: e202306497
30 Zheng J, Lu Z, Wu K, Ning GH, Li D. *Chem Rev*, 2020, 120: 9675–9742
31 Li H, Luo J, Zhang ZY, Wei RJ, Xie M, Huang YL, Ning GH, Li D. *Inorg Chem*, 2022, 61: 414–421
32 Li Y, Lei M, Gong L. *Nat Catal*, 2019, 2: 1016–1026
33 Lee W, Jung S, Kim M, Hong S. *J Am Chem Soc*, 2021, 143: 3003–3012
34 Zhou MJ, Zhang L, Liu G, Xu C, Huang Z. *J Am Chem Soc*, 2021, 143: 16470–16485
35 Yuan B, Mahor D, Fei Q, Wever R, Alcalde M, Zhang W, Hollmann F. *ACS Catal*, 2020, 10: 8277–8284
36 Zhao L, Cai W, Ji G, Wei J, Du Z, He C, Duan C. *Inorg Chem*, 2022, 61: 9493–9503
37 Zhang Z, Tang Z, Zhou Y, Wang P, Yang J, Zhu S. *Comput Theor Chem*, 2022, 1217: 113865
38 Mayer SF, Steinreiber A, Orru RVA, Faber K. *J Org Chem*, 2002, 67: 9115–9121
39 Liu J, Lam JWY, Tang BZ. *Chem Rev*, 2009, 109: 5799–5867
40 Zhu Y, Deng N, Feng M, Liu P. *Chin J Catal*, 2019, 40: 1505–1515
41 Sagadevan A, Charpe VP, Hwang KC. *Catal Sci Technol*, 2016, 6: 7688–7692
42 Xu H, Wu K, Tian J, Zhu L, Yao X. *Green Chem*, 2018, 20: 793–797
43 Duan H, Chen X, Yang YN, Zhao J, Lin XC, Tang WJ, Gao Q, Ning GH, Li D. *J Mater Chem A*, 2023, 11: 12777–12783
44 Wei RJ, You PY, Duan H, Xie M, Xia RQ, Chen X, Zhao X, Ning GH, Cooper AI, Li D. *J Am Chem Soc*, 2022, 144: 17487–17495
45 Wei RJ, Zhou HG, Zhang ZY, Ning GH, Li D. *CCS Chem*, 2021, 3: 2045–2053
46 Ouyang K, Hao W, Zhang WX, Xi Z. *Chem Rev*, 2015, 115: 12045–12090
47 Taylor RD, MacCoss M, Lawson ADG. *J Med Chem*, 2014, 57: 5845–5859
48 Charpe VP, Hande AA, Sagadevan A, Hwang KC. *Green Chem*, 2018, 20: 4859–4864
49 Kong Y, Wei K, Yan G. *Org Chem Front*, 2022, 9: 6114–6128